sustainability

MDPI

Article

Modeling, Simulation, and Performance Analysis of a Liquid-Infill Tunable Window

Xiaodong Wang [1,2], Yinan Yang [1,2], Xiaoyu Li [1,2] and Chunying Li [1,2,*]

[1] School of Architecture & Urban Planning, Shenzhen University, Shenzhen 518060, China
[2] Shenzhen Key Laboratory of Architecture for Health & Well-Being (in Preparation), Shenzhen 518060, China
* Correspondence: lichunyinghit@163.com

Abstract: Solar shading is important in buildings for better indoor thermal/light environment and energy conservation, especially in the tropical region. Compared with conventional windows with additional fixed shading devices, windows with adaptive self-shading functions take up less space and require less management labor. The present investigation focuses on a compact liquid-infill tunable window, which can provide adaptive shading with colored liquid-infill according to the surrounding environment. The numerical model of the liquid-infill tunable window was established on the basis of the law of energy and mass conservation, which enabled prediction of the adaptive response of the window under different boundary conditions. Then the thermal performance of this innovative window was analyzed in comparison with triple-layered clear glass windows. Influences of solar radiation level, incident angle, and ambient temperature were taken into consideration. The window was proven to be efficient in reducing indoor heat gain in the cooling season under strong solar radiation. With an 60° incident angle, the total indoor heat gain through window can be reduced by 1.60–8.33%. In the future, the established numerical model may be inserted into existing building simulation software as an energy-efficient window module to evaluate its energy and economic performance. The present study may inspire architectures and engineers in the design of near-zero energy and/or carbon neutral buildings.

Keywords: building energy conservation; solar shading; liquid-infill tunable window; numerical simulation

Citation: Wang, X.; Yang, Y.; Li, X.; Li, C. Modeling, Simulation, and Performance Analysis of a Liquid-Infill Tunable Window. *Sustainability* **2022**, *14*, 15968. https://doi.org/10.3390/su142315968

Academic Editors: Domenico Palladino and Iole Nardi

Received: 10 October 2022
Accepted: 21 November 2022
Published: 30 November 2022

1. Introduction

To cope with the energy crisis and climate change problem, energy saving in building is gaining extensive attention around the world [1]. According to statistical data, the primary energy consumption of the building sector accounted for approximately 20% of all commercial energy consumption. The total carbon emissions related to building energy use were approximately 2.2 billion tCO2 [2]. It is commonly recognized that buildings play an important role in energy conservation and carbon neutral realization. Due to the low thermal resistance of glass panes, windows are usually the weak point of thermal insulation, thus causing huge amount of energy consumption for indoor thermal regulation. For buildings in cooling-dominant regions, proper solar shading is recommended, as transmission of solar radiation influences not only indoor thermal and light environment but also energy consumption of air-conditioning system by a large scale [3,4]. Thermal and energy performances of various solar shading technologies have been a hot research topic in recent years, including the fixed shading devices, movable or adjustable shading devices, liquid-filled window, as well as adaptive shading glass or adaptive windows [5,6].

The fixed shading devices, including overhangs, horizontal/tilted/vertical louvers, flat panel devices, solar screens, and so on, are extensively investigated from the aspects of energy and economic performance, as well as structure optimization through both experiment measurements and numerical simulation [7,8]. On the other hand, movable or

adjustable shading devices are more attractive as they provide more flexible control of solar transmission under different outdoor conditions. Manually adjustable shading devices include venetian blinds, operable roller blinds, and movable roller shades permitting building occupants to create comfortable indoor environment accordingly to personal preferences [9,10]. Automatic control systems alter the solar transmission of shading devices according to preset schedule or triggering condition of indoor and/or outdoor, and provide preferable supplement to manual adjustment [11,12]. The adaptive shading control strategies are favorable from the aspect of building energy-saving, as occupants' regulation of shading devices tend to be influenced more by occupational dynamics (arrival and departure) than by the environmental conditions experienced over the day (such as work plane illuminance or transmitted solar radiation) and the occupants' regulation usually lags behind the change of environmental condition [13,14].

Comparatively, adaptive shading glass and windows are attracting increasingly more attention in recent decades, which realize sun blocking without extra devices or space occupation [15,16]. There are several types of dynamic glass, such as thermochromic [17], electrochromic [18], liquid crystals [19] as well as suspended particles device switchable glazing [20]. Multiple investigations were conducted to evaluate the energy-saving potential of thermally adaptive windows through experimental testing and numerical simulation. The study of Li and Zhu introduced transmittance-tuned thermochromic coatings for dynamic control of window thermal performance [21,22]. Jiang evaluated the energy performance of a thermo-responsive hydrogel window under the climate of Tucson, AZ, USA. The annual space-cooling energy was reduced by 8.1%, and 30.6 kWh/m^2 annual cooling energy-saving was achieved [23]. Aburas evaluated the energy performance of the nanoparticle thermochromic-coated glazing technology [24]. It was found that 7.1–46.4% annual energy-saving can be achieved in comparison with using an uncoated clear double-glazed window. Nakamura conducted an experimental study on the thermal performance of an HPC-AAm hydrogel window, and the indoor temperature was found to be reduced by 10 °C [25]. However, the above-mentioned technologies require advanced materials that are not commonly produced, which means the price might be very high and hinder the wide application. Overall speaking, the high-tech thermo-responsive windows are still in the state of research and testing, as the prolonged payback period hinders the large-scale application.

On the other hand, the adaptive shading water-flow window utilizes colored liquid within cavities between the glass panes as solar shading. The circulating liquid between the window cavity and the additional heat exchanger performs as a solar collection medium to reduce indoor cooling load and preheats domestic hot water at the same time [26,27]. The alteration of the window shading coefficient is realized by changing the pigment concentration within the liquid, which brings about continuous adjustment of solar transmission. Li studied a double-circulation water-flow window with adaptive shading control through dynamic modeling. Results showed year-round solar energy collection efficiency of 17.95–21.06% and indoor heat gain reduction of 50% compared with common double-layer window [28]. However, the water-flow window requires a complicated pipework system. This drawback makes it almost impossible to apply water-flow windows in existing buildings. Moreover, the pipework and periodic maintenance requirement would increase both initial investment and operation cost.

Under such circumstances, the innovative concept of low-cost liquid-infill tunable window was proposed by Fazel [29]. The comprehensive shading rate can respond to the surrounding environment automatically on the basis of the basic law of thermodynamics. Similar to the water-flow window, the tunable window also employs colored liquid as a sunshade to control solar transmittance and indoor heat gain; the adaptive shading mechanism is presented in Figure 1.

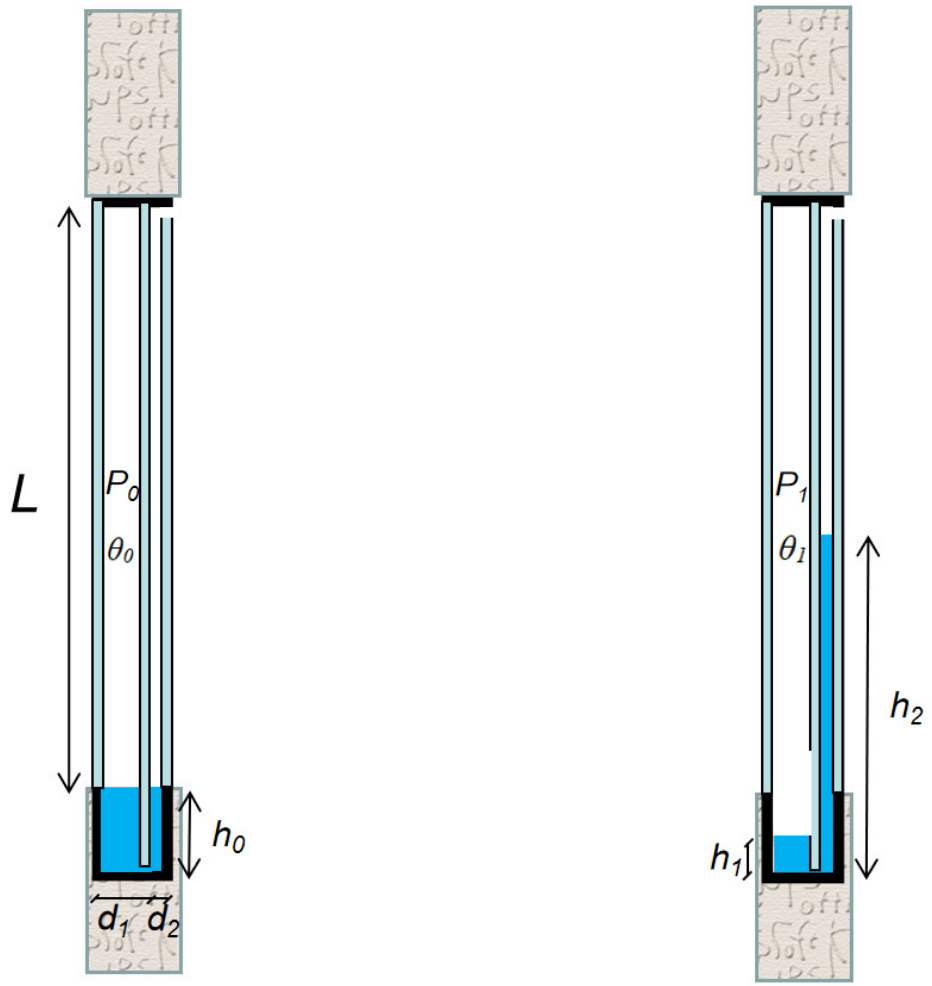

Figure 1. Schematic structure of the liquid-infill tunable window. (**a**) Initial state. (**b**) Transformed state.

With a similar outlook as the common window, liquid-infill tunable window is composed of three parallel glass panes forming two cavities. There is colored liquid at the bottom of the window, which traps air in the closed left-side cavity. Meanwhile, the right-side cavity is connected to the atmosphere and maintains the same air pressure with the surrounding environment. Positioned in an external wall, the trapped air expands under higher temperatures, and pushes the colored liquid to climb in the right-side window cavity, which is much thinner compared with the left-side one. In contrast with conventional fixed or adjustable shading devices attached on building windows, this compact adaptive shading window is more attractive because of the decreased first investment, lessened space occupation, and lower operation cost and management labor.

Considering the huge demand for building energy conservation and the above-mentioned advantages, the application potential of this tunable window is quite promising. However, there is not enough fundamental information presented in existing investigation. Thus, the window is not getting much attention from the green building industry, let alone application in real projects. In the research work of [29], energy performance of this liquid-infill tunable window was numerically analyzed with the aid of commercial simulation software Ecotect (by Autodesk, Portland, US). The simulation results showed a substantial reduction in both heating and cooling energy consumption. However, the heat transfer coefficient of the entire window was taken as constant in the simulation. In this way, the influence of variant height of the liquid layer to the comprehensive heat transfer through

the window was omitted. In other words, the thermal insulation of this window should be dependent on both indoor and outdoor environment, which may not be conveniently realized with existing mainstream simulation software. Meanwhile, the height of the liquid in the right-side cavity was assumed to be dependent on the room temperature in [29]. Considering that the height of the liquid should be more dependent on the temperature of the trapped air, it is influenced by both the outdoor and indoor environment and is usually higher than the room temperature during the cooling season.

In summary, this energy-efficient adaptive window can provide sun-blocking flexibly without energy consumption or manual labor. The precise prediction of its thermal responses under different boundary conditions are worthy of study, which is carried out in the present investigation with a self-developed FORTAN program. Firstly, the numerical model of this window is built on the basis of the law of energy and mass conservation. By solving the equations, the temperatures of the trapped air, glass panes, liquid layers, as well as the heights of the liquid layers in both cavities can be calculated. In this way, the heat transfer through the window can be ascertained. Afterwards, the thermal performance of this innovative window under different environmental conditions are analyzed. Influences of solar irradiation, incident angle, and ambient temperature are taken into consideration.

The simulation results may provide basic information to engineers in the green building industry for decision-making of energy-efficient window design. Additionally, the established numerical model may be inserted in commercial software as a module and be used for the energy and economic performance prediction of this adaptive window in real projects. The organizational structure of this paper is as follows: (1) the background of this investigation; (2) introduction of the numerical model; (3) illustration of the simulation cases; (4) analysis of simulation results; (5) discussions and future works; and (6) conclusions.

2. Numerical Model

A numerical model of the liquid-infill tunable window under investigation was established and utilized to evaluate its performance under different boundary conditions. The incident solar radiation on the window surface, which is an important indoor heat source during the cooling season, should be carefully accounted for in the design of any transparent building envelop. Accordingly, the solar energy flow path within the adaptive shading window and heat transfer mechanism between the glass panes and adjacent indoor/outdoor environment is illustrated in Figure 2.

The numerical model of the window was set up on the basis of mass and energy conservation, which is demonstrated as Equations (1)–(22). Equation (1) describes the mass conservation of the colored liquid within the window cavities. Equation (2) represents the ideal gas law of the trapped air in the left-side window cavity, and Equations (3)–(8) are developed on the basis of energy conservation of the incident solar radiation, in which the window is divided into two parts: the top part consisting of three layers of clear glass without liquid layer and the lower part consisting of three layers of clear glass with liquid layer in the cavity. The separate calculation is necessary since the optical and thermal properties of these two parts of the window are different. This issue should be taken into consideration in building simulation software as well as when this numerical model is to be inserted as a window module. Equations (9)–(22) present the convective and radiative heat transfer between the innermost and outermost glass panes and surrounding indoor and outdoor environment. Similarly, the calculation is dealt with separately for the top part and the lower part of the liquid tunable window.

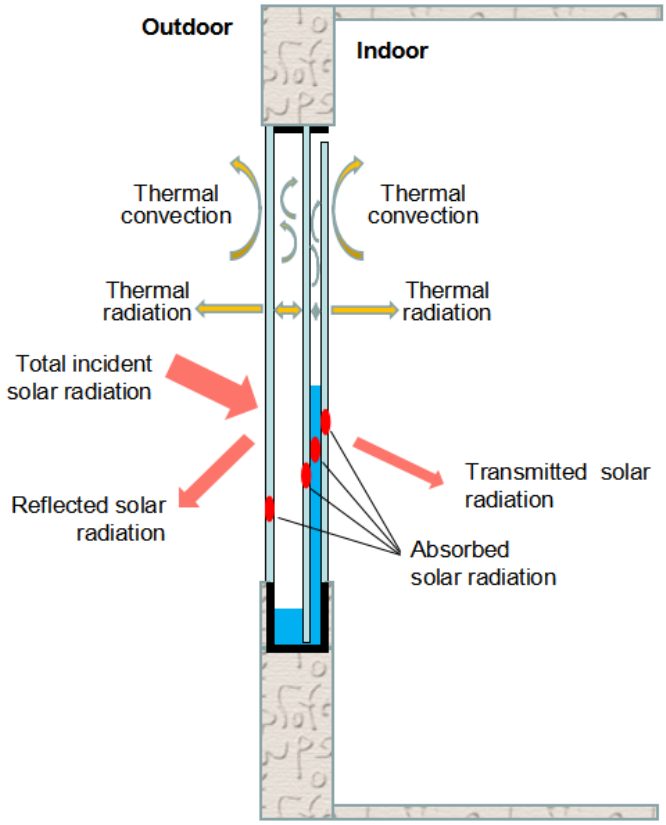

Figure 2. Solar energy flow path and heat transfer mechanism within the liquid-infill tunable window.

$$h_0(d_1 + d_2) = h_1 \cdot d_1 + h_2 \cdot d_2 \tag{1}$$

where

h_0, the height of the liquid in the initial state, as shown in Figure 1a, m;

h_1, h_2, the heights of the liquid in the left-side and the right-side cavities in the transformed state, as shown in Figure 1b, m;

d_1, d_2, the thicknesses of the left-side and the right-side cavities, respectively, m;

$$\frac{P_0 \cdot V_0}{\theta_0} = \frac{P_1 \cdot V_1}{\theta_1} = \frac{P_0 \cdot (L - h_0) \cdot W \cdot d_1}{\theta_0} = \frac{(\rho \cdot g \cdot (h_2 - h_1) + P_0) \cdot (L - h_1) \cdot W \cdot d_1}{\theta_1} \tag{2}$$

where

P_0, the air pressure within the left-side cavity in the initial state, which is the same as ambient environment and is taken as 100,325 Pa in the present investigation, Pa;

P_1, the air pressure within the left-side cavity in the transformed state, as shown in Figure 1b, Pa;

V_0, V_1, the volumes of air within the left-side cavity in the initial state and the transformed state, respectively, m^3;

θ_0, θ_1, the absolute temperatures of air within the left-side cavity in the initial state and the transformed state, respectively, K;

L, W, the height and width of the window, respectively, W;

ρ, the density of the liquid within the window, kg/m^3;

g, the gravitational constant, m/s^2;

$$G_{Total}^{top} = G_{ref}^{top} + G_{trans}^{top} + G_{abs}^{top} = G_{ref}^{top} + G_{trans}^{top} + Q_1^{top} + Q_2^{top} + Q_3^{top} + Q_4^{top} \tag{3}$$

$$G_{Total}^{lower} = G_{ref}^{lower} + G_{trans}^{lower} + G_{abs}^{lower} = G_{ref}^{lower} + G_{trans}^{lower} + Q_1^{lower} + Q_2^{lower} + Q_3^{lower} + Q_4^{lower} \tag{4}$$

where

G_{Total}^{top}, the total incident solar radiation on the top part of the window with no liquid layer, *W*;

G_{Total}^{lower}, the total incident solar radiation on the lower part of the window with liquid layer, *W*;

G_{ref}^{top}, the reflected solar radiation at the outside surface of $g1$ (the external glass pane) on the top part of the window with no liquid layer, *W*;

G_{ref}^{lower}, the reflected solar radiation at the outside surface of $g1$ (the external glass pane) on the lower part of the window with liquid layer, *W*;

G_{trans}^{top}, the solar radiation transmitted through the top part of the window with no liquid layer to indoor, *W*;

G_{trans}^{lower}, the solar radiation transmitted through the lower part of the window with liquid layer to indoor, *W*;

G_{abs}^{top}, the solar radiation absorbed by the glass panes within the top part of the window, *W*;

G_{abs}^{lower}, the solar radiation absorbed by the glass panes and colored liquid within the lower part of the window, *W*;

Q_1^{top}, Q_1^{lower}, the convective heat flows from outside surface of $g1$ (the external glass pane) back to the ambient environment at the top part and the lower part of the window, respectively, *W*;

Q_2^{top}, Q_2^{lower}, the convective heat flows from the indoor surface of $g3$ (the internal glass pane) to room space at the top part and the lower part of the window, respectively, *W*;

Q_3^{top}, Q_3^{lower}, the radiative heat flows from the outdoor surface of $g1$ (the external glass pane) to environment that includes the sky and surrounding solid surfaces at the top part and the lower part of the window, respectively, *W*;

Q_4^{top}, Q_4^{lower}, the radiative heat flows from the indoor surface of $g3$ (the internal glass pane) to room surfaces at the top part and the lower part of the window, respectively, *W*;

From Equation (3), the total incident solar radiation (G_T) is partly reflected (G_{ref}), partly transmitted (G_{trans}) to indoor, and partly absorbed (G_{abs}) by the glass panes and liquid volume.

$$G_{ref}^{top} = \gamma^{top} \cdot G_{Total}^{top} \tag{5}$$

$$G_{ref}^{lower} = \gamma^{lower} \cdot G_{Total}^{lower} \tag{6}$$

$$G_{trans}^{top} = \tau^{top} \cdot G_{Total}^{top} \tag{7}$$

$$G_{trans}^{lower} = \tau^{lower} \cdot G_{Total}^{lower} \tag{8}$$

where

γ^{top}, γ^{lower}, the comprehensive reflectance at the top part and the lower part of the window, respectively, -;

τ^{top}, τ^{lower}, the comprehensive transmittance of the window at the top part and the lower part, respectively, -;

The absorbed energy is stored either within the glass panes or liquid volume or is transferred to the adjacent indoor/outdoor environment. In the present investigation, the adaptive shading window is assumed to maintain a heat balance state. Therefore, the temperature of both glass panes and liquid volume are constant, and this is why no thermal storage is taken into consideration in Equation (3).

$$Q_1^{top} = A^{top} \cdot h_{c,1a}^{top} \cdot (T_{g1}^{top} - T_a) \tag{9}$$

$$Q_1^{lower} = A^{lower} \cdot h_{c,1a}^{lower} \cdot (T_{g1}^{lower} - T_a) \tag{10}$$

$$Q_2^{top} = A^{top} \cdot h_{c,3rm}^{top} \cdot (T_{g3}^{top} - T_{rm}) \tag{11}$$

$$Q_2^{lower} = A^{lower} \cdot h_{c,3rm}^{lower} \cdot (T_{g3}^{lower} - T_{rm}) \tag{12}$$

$$Q_3^{top} = A^{top} \cdot h_{r,1a}^{top} \cdot (T_{g1}^{top} - T_a) \tag{13}$$

$$Q_3^{lower} = A^{lower} \cdot h_{r,1a}^{lower} \cdot (T_{g1}^{lower} - T_a) \tag{14}$$

$$Q_4^{top} = A^{top} \cdot h_{r,3rm}^{top} \cdot (T_{g3}^{top} - T_{rm}) \tag{15}$$

$$Q_4^{lower} = A^{lower} \cdot h_{r,3rm}^{lower} \cdot (T_{g3}^{lower} - T_{rm}) \tag{16}$$

where

A^{top}, A^{lower}, the cross-sectional areas of the top part and the lower part of the window, respectively, m^2;

T_{g1}^{top}, T_{g1}^{lower}, T_3^{top}, T_3^{lower}, the temperatures of external glass pane $g1$ and internal glass pane $g3$ at the top part and the lower part of the window, respectively, $^\circ C$;

T_a, T_{rm}, the temperatures of ambient environment and indoor air (which is assumed to be equivalent to the indoor solid surfaces) at the top part and the lower part of the window, respectively, $^\circ C$;

$h_{c,1a}^{top}$, $h_{c,1a}^{lower}$, the convective heat transfer coefficients between external glass pane $g1$ and ambient environment at the top part and the lower part of the window, respectively, $W/(m^2 \cdot ^\circ C)$;

$h_{c,3rm}^{top}$, $h_{c,3rm}^{lower}$, the convective heat transfer coefficients between the internal glass pane $g3$ and indoor air at the top part and the lower part of the window, respectively, $W/(m^2 \cdot ^\circ C)$;

$h_{r,1a}^{top}$, $h_{r,1a}^{lower}$, the radiative heat transfer coefficients between the glass pane $g1$ and ambient environment at the top part and the lower part of the window, respectively, $W/(m^2 \cdot ^\circ C)$;

$h_{r,3rm}^{top}$, $h_{r,3rm}^{lower}$, the radiative heat transfer coefficients between the internal glass pane $g3$ and solid indoor surfaces at the top part and the lower part of the window, respectively, $W/(m^2 \cdot ^\circ C)$;

The heat transfer coefficients at window surfaces are calculated on the basis of empirical formulas [30], and are listed as follows:

$$h_{c,1a}^{top} = h_{c,1a}^{lower} = 2.8 + 3.0 v_{wind} \tag{17}$$

$$h_{r,1a}^{top} = \frac{\sigma((\theta_a^{top})^2 + (\theta_{g1}^{top})^2)(\theta_a^{top} + \theta_{g1}^{top})}{\frac{1}{\varepsilon_a} + \frac{1}{\varepsilon_{g1}} - 1} \tag{18}$$

$$h_{r,1a}^{lower} = \frac{\sigma((\theta_a^{lower})^2 + (\theta_{g1}^{lower})^2)(\theta_a^{lower} + \theta_{g1}^{lower})}{\frac{1}{\varepsilon_a} + \frac{1}{\varepsilon_{g1}} - 1} \tag{19}$$

$$h_{c,3rm}^{top} = h_{c,3rm}^{lower} = 4.3 \tag{20}$$

$$h_{r,3rm}^{top} = \frac{\sigma((\theta_{g3}^{top})^2 + (\theta_{rm}^{top})^2)(\theta_{g3}^{top} + \theta_{rm})}{\frac{1}{\varepsilon_{g3}} + \frac{(1-\varepsilon_{rm})(H_{rm}+W_{rm})}{\varepsilon_{rm} \cdot 2(H_{rm}W_{rm}+H_{rm}L_{rm}+L_{rm}W_{rm})}} \tag{21}$$

$$h_{r,3rm}^{lower} = \frac{\sigma((\theta_{g3}^{lower})^2 + (\theta_{rm}^{lower})^2)(\theta_{g3}^{lower} + \theta_{rm})}{\frac{1}{\varepsilon_{g3}} + \frac{(1-\varepsilon_{rm})(H_{rm}+W_{rm})}{\varepsilon_{rm} \cdot 2(H_{rm}W_{rm}+H_{rm}L_{rm}+L_{rm}W_{rm})}} \tag{22}$$

where

v_{wind}, the wind speed at the outside surface of $g1$ (the external glass pane), m/s;

θ_{g1}^{top}, θ_{g1}^{lower}, θ_{g3}^{top}, θ_{g3}^{lower}, the absolute temperatures of $g1$ and $g3$ at the top part and the lower part of the window, respectively, K;

θ_a, θ_{rm}, the absolute temperatures of the ambient environment and room surfaces (assumed the same as indoor air temperature), K;

σ, the Stefan–Boltzmann constant, 5.67×10^{-8} $W/(m^2 \cdot K^{-4})$;

ε_a, ε_{g1}, ε_{g3}, ε_{rm}, the emissivity measures of ambient environment, outside surface of $g1$ (the external glass pane), inside surface of $g3$ (the internal glass pane), and indoor envelop surfaces, -; and

H_{rm}, W_{rm}, L_{rm}, the height, width, and length of the adjacent room, respectively, m.

3. Performance Simulation

3.1. Room and Window Configurations

The liquid-infill tunable window is assumed to be applied to an air-conditioned room with dimensions of 3.0 m (*Length*) × 3.0 m (*Width*) × 3.0 m (*Height*). The indoor temperature is preset to be 26 °C during the cooling season, which is recommended by Chinese government regulations for the purpose of energy conservation. The size of the south-oriented vertical window is 1.0 m (*Width*) × 1.0 m (*Height*), with an initial liquid depth (h_0) of 0.2 m. It should be noted that initially the liquid is hidden within the wall beneath the window, as illustrated in Figure 2. This hidden part is assumed to be well-insulated and is not taken into consideration in the heat transfer calculation.

The three glass panes of the liquid-infill tunable window are common clear glass with a unified thickness of 0.006 m. Consequently, the first investment would be quite competitive compared with other adaptive window designs, considering neither expensive thermochromic glazing nor extra shading devices are applied. The optical properties of the glass panes are obtained from software Window [31] and listed in Table 1.

Table 1. Properties of the clear glass pane in the window [31].

Glazing ID	01_Clear_6.syp
Thickness (m)	0.006
Solar transmittance at normal incidence	0.804
Solar reflectance at normal incidence (front side)	0.074
Solar reflectance at normal incidence (back side)	0.074
Emissivity (front side)	0.84
Emissivity (back side)	0.84

As for the internal structure of the window, the thickness of the right-side cavity (d_2) should not be too small or else it would be hard to control the accuracy during window manufacturing. In addition, unfavorable liquid block might form during the decline of the liquid layer when temperature of the trapped air descends. Meanwhile, d_2 should not be too large so that the window does not become too bulky, resulting in trouble in transportation and installation. In addition, the thick liquid layer tends to impose excessive pressure to the adjacent glass panes, which would make the glass panes transform adversely, especially in the center of the window. According to the authors' experience acquired from water-flow window experiments described in [32], d_2 is set as 0.01 m, which is an appropriate thickness for the shading liquid layer. The thickness of the left-side cavity d_1 is taken as 0.12 m, which means the entire thickness of the proposed adaptive shading window is 0.148 m.

The density of the liquid would significantly influence the effect of sunshade, as the height of the shading liquid layer under different conditions is directly dependent on it. At the same time, the solar transmittance of the liquid layer is a decisive factor of the comprehensive shading coefficient. In the present investigation, density of the liquid was set as 120.0 kg/m^3. In practice, different types of liquid materials can be mixed together to achieve the designated density according to the climate and solar shading requirements. Meanwhile, the solar transmittance of mixed liquid layer was preset as 0.6 with thickness of 0.01 m. The transmittance is adjustable through the addition of pigments of different

properties and concentrations to the liquid. In real application, the shading coefficient of the window as a whole can be modified flexibly in a relatively wide range, according to specific demand.

In the present investigation, the adaptive movement of the liquid within the adaptive shading window was preset to begin when ambient temperature exceeds 26 °C, i.e., when there is an inward heat transfer caused by a temperature difference where solar energy transmission would cause unfavorable indoor heat gain, which would need to be removed. Accordingly, there is a temperature-controlled switch at the top of the window, which is normally open and causes the air in the left-side cavity to remain in connection with ambient atmosphere. When ambient air temperature exceeds 26 °C, the switch automatically closes and air is trapped within the left-side cavity. At that point, the window provides sun-blocking by the shading liquid layer in the right-side cavity.

3.2. Simulation Cases

The thermal performance of the liquid-infill tunable window (adaptive shading case, in short) is evaluated through numerical simulation, in comparison with the common triple-layer clear glass window (non-shading case, in short) under different environmental conditions. The outdoor temperature is set to be in the range from 20 to 32 °C with intervals of 3 °C, which represents the typical outdoor temperature variance in the cooling season. In total, nine combinations of incident solar radiation are considered. The global solar irradiance levels are 1000, 650, and 300 W/m^2, with incident angles of 60, 30, and 0°. For the south-oriented vertical window, the incident beam and diffused solar radiation values are listed in Table 2, which are calculated on the basis of formulas in [33].

Table 2. Incident solar radiation combinations of comparative cases.

Combination No.	Global Solar Irradiance (W/m^2)	Incident Angle (°)	Total Incident Solar Energy (W/m^2)	Incident Beam Solar Energy (W/m^2)	Incident Diffused Solar Energy (W/m^2)
1	1000	60	597	390	207
2	650	60	442	115	327
3	300	60	223	5	218
4	1000	30	865	675	189
5	650	30	521	199	322
6	300	30	227	9	217
7	1000	0	946	780	166
8	650	0	545	230	315
9	300	0	228	11	217

In summary, the liquid-infill tunable window is simulated under five outdoor/indoor temperature combinations with nine incident solar radiation conditions. As a result, there are 45 different boundary conditions. The simulation was repeated for liquid-infill tunable window (adaptive shading case) and triple-layer clear glass window (non-shading case) with the same window size, orientation, and boundary conditions.

Numerical simulation was carried out with a self-developed FORTRAN program based on the physical model described in Section 2. For each simulation run, the distributions of incident solar energy, including reflected, transmitted, as well as absorbed within glass panes and liquid layers, are calculated according to the optical properties. Then, the equations are solved, and the values of h_1, h_2, and θ_1 under the specific indoor/outdoor condition are acquired. The internal glass pane temperature is calculated on the basis of the principle of heat balance simultaneously. Together with the heat transfer coefficient of the internal glass pane with the room, as well as the direct solar transmission, the total indoor

heat gain/loss through the window can be predicted. As for the triple-layer clear glass window, the calculation process was carried out similarly but without the participation of colored liquid layer.

4. Simulation Results

4.1. Window Performance under Different Irradiance Conditions

The performance of the liquid-infill tunable window was compared with that of the triple-layer clear glass window under different solar irradiance conditions with outdoor and indoor air temperatures fixed to be 32 °C and 26 °C, as show in Figures 3–6. Figure 3 shows the total incident solar radiation on the vertical window (the blue dotted line) and the height of the shading liquid layer within the right-side window cavity (the black solid line).

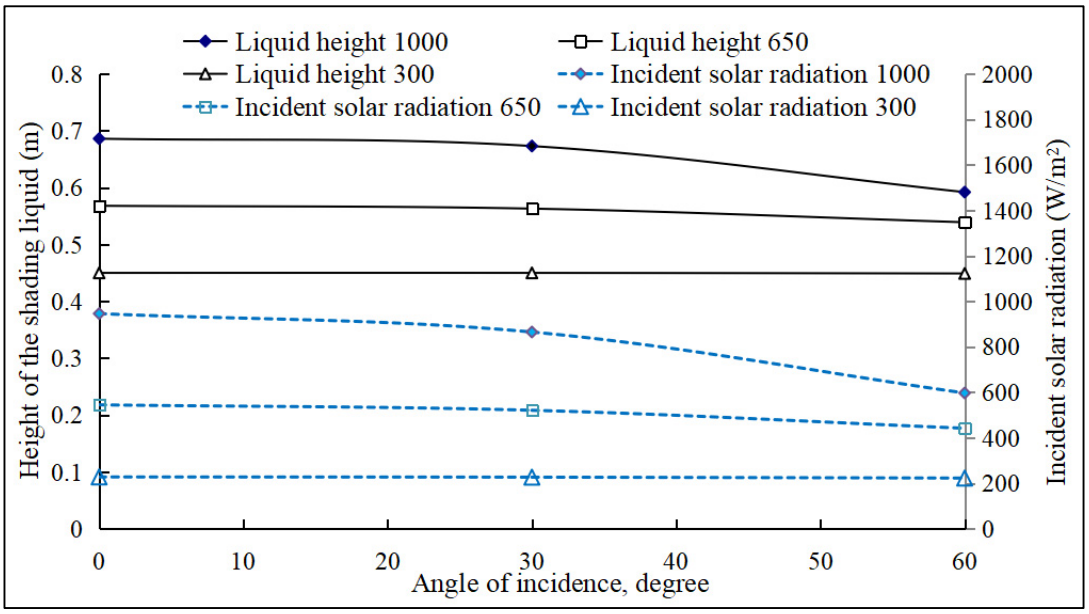

Figure 3. Heights of the shading liquid layer under different solar irradiance conditions.

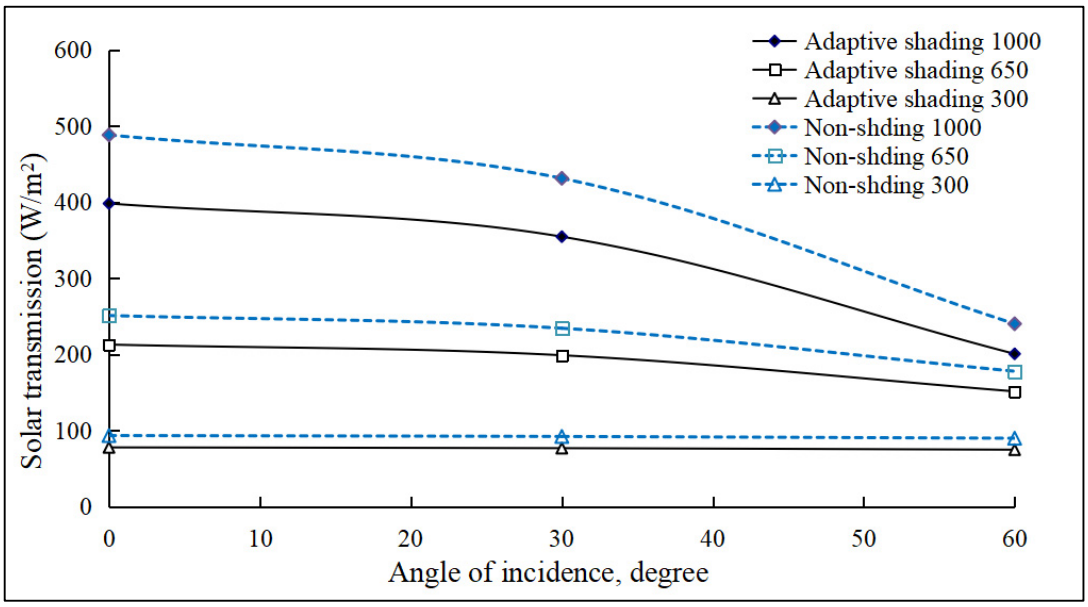

Figure 4. Directly transmitted solar energy through the window under different solar irradiance conditions.

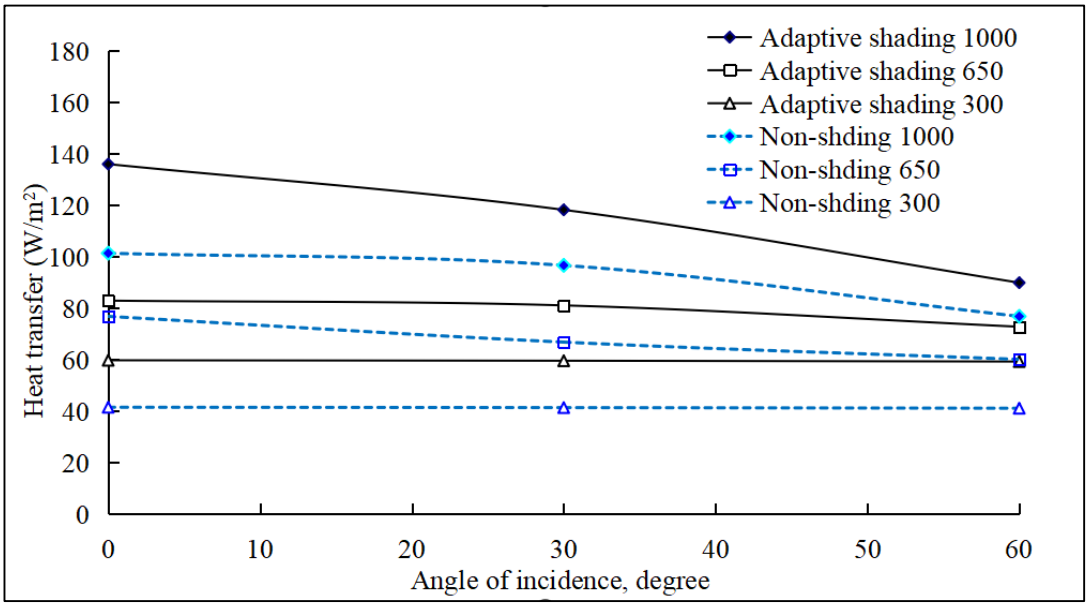

Figure 5. Convective and radiative heat transfer from the window to the room under different solar irradiance conditions.

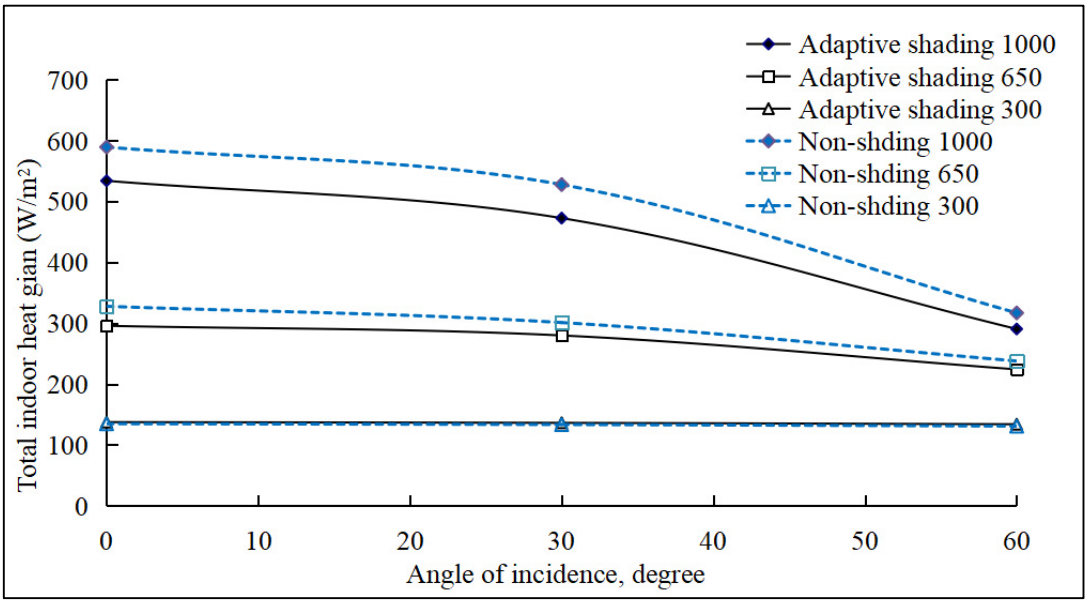

Figure 6. Total indoor heat gain through the window under different solar irradiance conditions.

With same global solar irradiance level, the incident angle influences the accepted solar energy largely. As seen in Figure 3, the 1.0 m^2 south-oriented vertical window accepted, respectively, 597, 865, and 946 W/m^2 solar energy at 60°, 30°, and 0° incident angles with 1000 W/m^2 global solar irradiance level. The larger incident angle of 60° resulted in the least incident solar energy, which was only 63.1% of that of the 0° incident case. As for the 650 and 300 W/m^2 global solar irradiance levels, the differences of accepted solar energy under different incident angles were smaller. For the 650 W/m^2 level, the incident solar radiation values at 60° incident angle and 0° incident angle were within a 20% difference. For the 300 W/m^2 level, the incident solar radiation values at 60° incident angle and 0° incident angle were very close, with merely a 2.2% difference.

As shown in Figure 3, the heights of the shading liquid were in the range of 0.45–0.69 m for the nine cases under discussion. With the same indoor and outdoor temperatures, the variances of liquid movement within the window cavities were caused solely by the

difference of incident solar energy. With more solar energy incident, the temperature of the trapped air within the left-side window cavity (as shown in Figure 2) is supposed to be higher with more heat absorption from adjacent glass panes, which results in a higher pressure to push more liquid to the right-side window cavity. Thus, superior solar shading is provided under stronger solar irradiance, which is positive for cooling load reduction and building energy conservation in the cooling season. Accordingly, the heights of the shading liquid layer were, respectively, 0.69, 0.67, and 0.59 m under 946, 865, and 597 W/m^2 incident solar energy.

Figure 4 shows the transmitted solar energy through the window in the adaptive shading case and non-shading case under different irradiance conditions. Figure 5 shows the conductive and radiative heat transfer from the window to the room. The total indoor heat gain/loss through the window is the sum of conductive/radiative heat gain/loss and direct solar transmission, which is displayed in Figure 6. In Figures 4–6, the number in the figure legend represents the global irradiance level. The outdoor and indoor air temperatures remained at 32 °C and 26 °C.

In Figure 4, the blue dotted lines represent the transmitted solar energy through the triple-layer clear glass window without shading under different conditions, which was always above the liquid-infill tunable window, i.e., the black solid lines. With solar shading provided by the colored liquid layer in the right-side window cavity, part of the incident solar energy was blocked, and the indoor heat gain from solar transmission was reduced, thus preventing the excessive indoor heat gain through the window. The reduction was larger when solar irradiance was stronger, which is reasonable since the shading liquid layer was higher. For example, when the global solar irradiance level was 1000 W/m^2 and the incident angle was 0°, the transmitted solar radiation was reduced from 488.1 W/m^2 (non-shading window) to 398.1 W/m^2 (liquid-infill tunable window). The equivalent solar transmission rate was 0.516 for the non-shading window and 0.421 for the liquid-infill tunable window, with a 18.5% reduction. As for the 30° and 60° incident angles, the solar transmissivity reduced from 0.498 to 0.410 and from 0.402 to 0.336, respectively. The corresponding reductions decreased slightly, which were 17.8% and 16.5%, respectively.

Meanwhile, the observed differences between adaptive shading case and non-shading case were smaller when global irradiance level was 300 W/m^2. The comprehensive transmissivity of the triple-layer clear glass window was within the range of 0.402–0.409 at different incident angles. As for the liquid-infill tunable window, the transmissivity fell into the range of 0.334–0.340. The corresponding reductions caused by the liquid layer were quite similar, approximately 16.7% under different incident angles.

In Figure 5, the blue dotted lines remained below the black solid lines, representing the effect that the indoor heat gain from convective and radiative heat transfer between the window and the room was always larger for the adaptive shading cases. This was because of the smaller thermal insulation of liquid-infill tunable window in which the air in the right-side window cavity was partly replaced with liquid, which benefits heat flow from outdoor to indoor. For the cases with 1000 W/m^2 global irradiance level, the convective and radiative heat transfer increased from 101.4 W/m^2 (non-shading window) to 136.1 W/m^2 (adaptive-shading window) at the 0° incident angle, from 96.7 W/m^2 to 118.3 W/m^2 at the 30° incident angle, and from 76.9 W/m^2 to 90.0 W/m^2 at the 60° incident angle. The increments were, respectively, 34.6%, 21.6%, and 13.1%. As for the cases with weaker irradiance levels, the increments were quite similar under different incident angles.

In summary, the liquid layer in the liquid-infill tunable window contributeed to solar heat blocking while performing negatively in thermal insulation. Figure 6 shows the comprehensive indoor heat gain through the window under different conditions.

In Figure 6, the solar heat block effect is in prominence under 1000 W/m^2 and 650 W/m^2 global irradiance conditions, resulting in a smaller indoor heat gain with the liquid-infill tunable window. When global solar irradiance level was as high as 1000 W/m^2 and the incident angle was 0°, the total indoor heat gain reduced from 589.6 W/m^2 (non-shading window) to 534.1 W/m^2 (liquid-infill tunable window). The reduction percentage

was 9.4%. As for the 650 W/m^2 global irradiance level, the reduction percentage was relatively smaller, which was 9.8%. However, the indoor heat gain increased from 134.7 W/m^2 to 137.4 W/m^2, i.e., increased by 2.0% when global solar irradiance level was 300 W/m^2 and incident angle was 0°. This was caused by the higher level of convective/radiative heat transfer between the inner glass pane and indoor environment in the adaptive shading window case. Similarly, the indoor heat gain increased by 2.1% and 2.4% with global solar irradiance level of 300 W/m^2 and incident angles of 30° and 60°.

4.2. Window Performance under Different Ambient Temperatures

The performance of the liquid-infill tunable window was compared with the triple-layer clear glass window under different outdoor/indoor temperature combinations, as illustrated in Figures 7–10. Figure 7 shows the heights of the shading liquid layer under different conditions. The numbers in the figure legend represent the global irradiance level and incident angle to the window. Figures 8–10 show the direct solar transmission through the window, inward convective and radiative heat transfer, and the comprehensive indoor gain through the window, respectively. The solar incident angle was fixed at 60°, which was more frequently observed for a vertical window compared with the 0° or 30° incident angles.

In Figure 7, the shading liquid within the left-side window cavity rises under higher outdoor temperature and stronger solar irradiance. As mentioned above, the temperature-control switch seals the left-side window cavity when ambient temperature is below 26 °C. Therefore, the shading liquid remained at the "initial state", as shown in Figure 1a, with ambient temperatures of 20 °C and 23 °C. The height of the shading liquid was 0.0 m under such conditions. Therefore, the performance of the present adaptive liquid-shading window remained the same as the common triple-layer window. In practical applications, the window should be redesigned according to the specific indoor air temperature. For example, if the preset temperature of indoor air temperature were 24 °C, the window should be designed to take action (provide liquid shading) when ambient temperature exceeds 24 °C. In this way, the indoor heat gain from ambient temperature can be minimized to the largest extent and more cooling energy can be reduced.

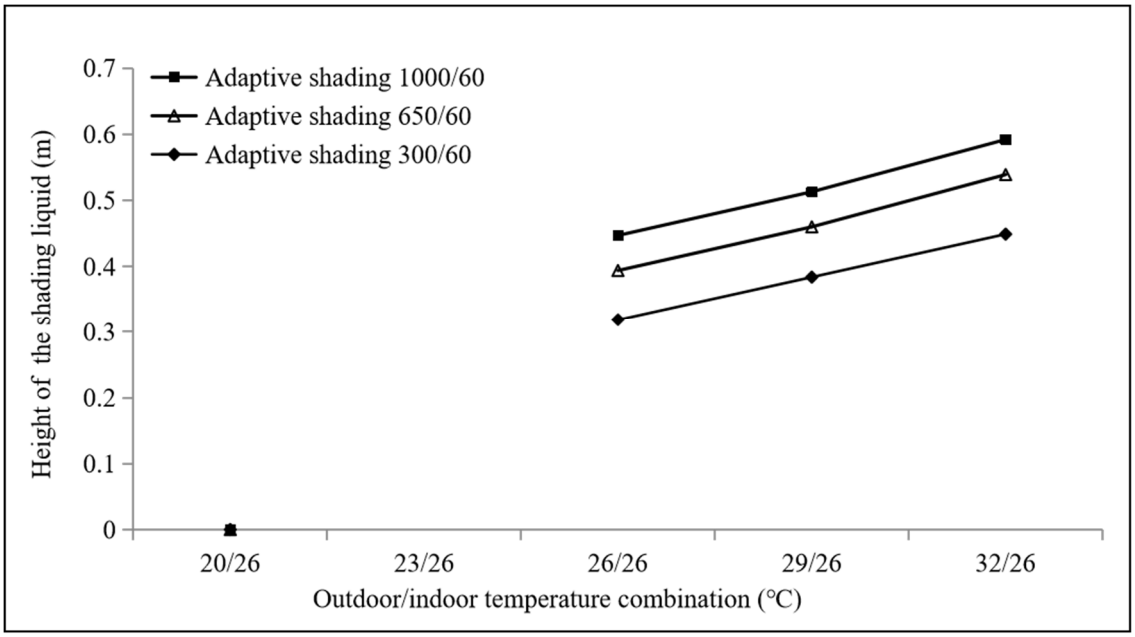

Figure 7. Heights of the shading liquid layer under different outdoor/indoor temperature combinations.

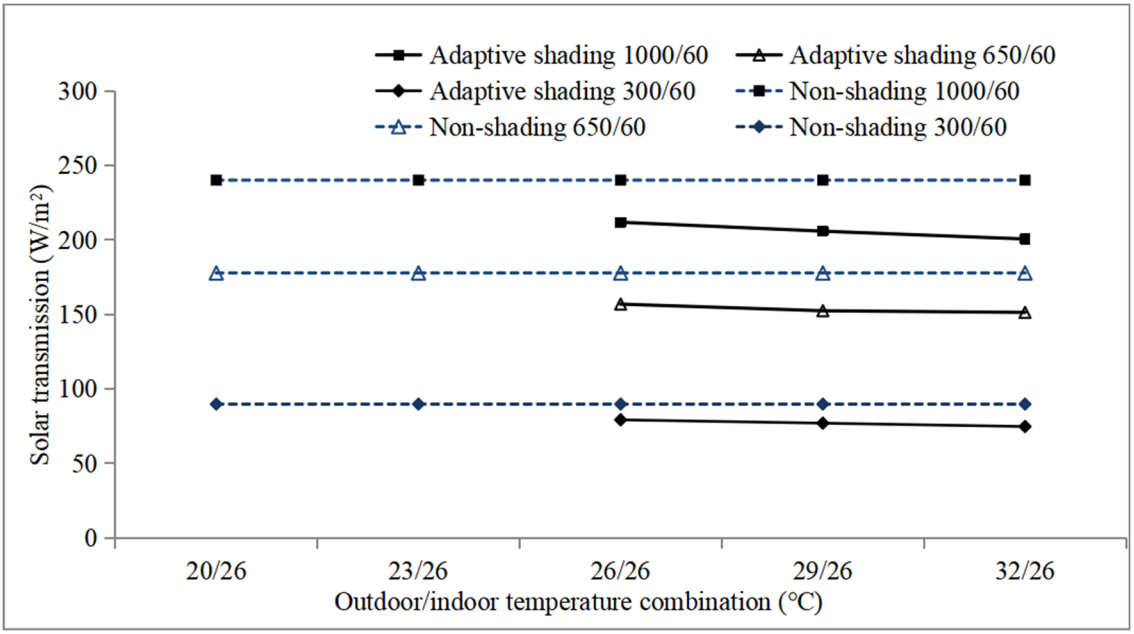

Figure 8. The direct solar energy transmission through window under different outdoor/indoor temperature combinations.

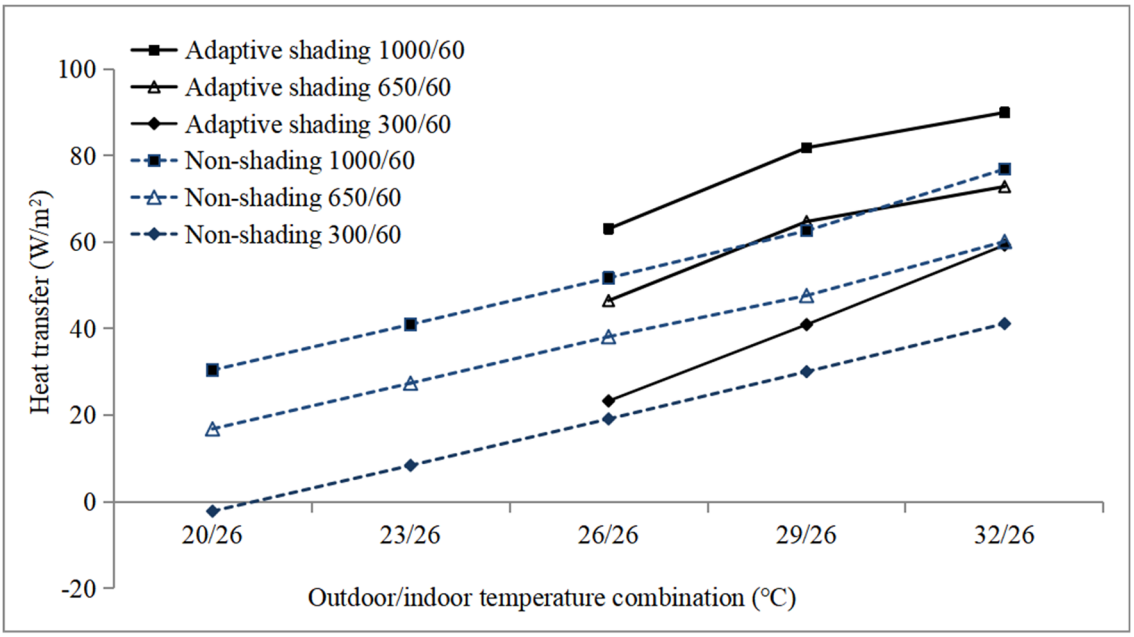

Figure 9. The convective and radiative heat transfer from window to indoor under different outdoor/indoor temperature combinations.

On the contrary, the temperature-control switch permits the liquid to flow from the bottom to the right-side cavity due to the increased pressure of the trapped air within the left-side window cavity when outdoor temperature exceeds 26. The higher ambient temperature and stronger solar radiation resulted in larger air pressure within the left-side cavity, thus pushing more liquid to the right-side window cavity to provide better shading. The highest level of the liquid layer was 0.592 m, when outdoor temperature was as high as 32 °C and global solar irradiance level was 1000 W/m^2. When outdoor temperature decreased to 26 °C, the height of the shading liquid was reduced to 0.447 m. This means, with the specific solar incident level and angle, the liquid layer rose by approximately

0.024 m with every 1 °C outdoor temperature increment. Meanwhile, the heights of the liquid layer were 0.539 m and 0.449 m under 650 W/m^2 and 300 W/m^2 global irradiance levels, respectively.

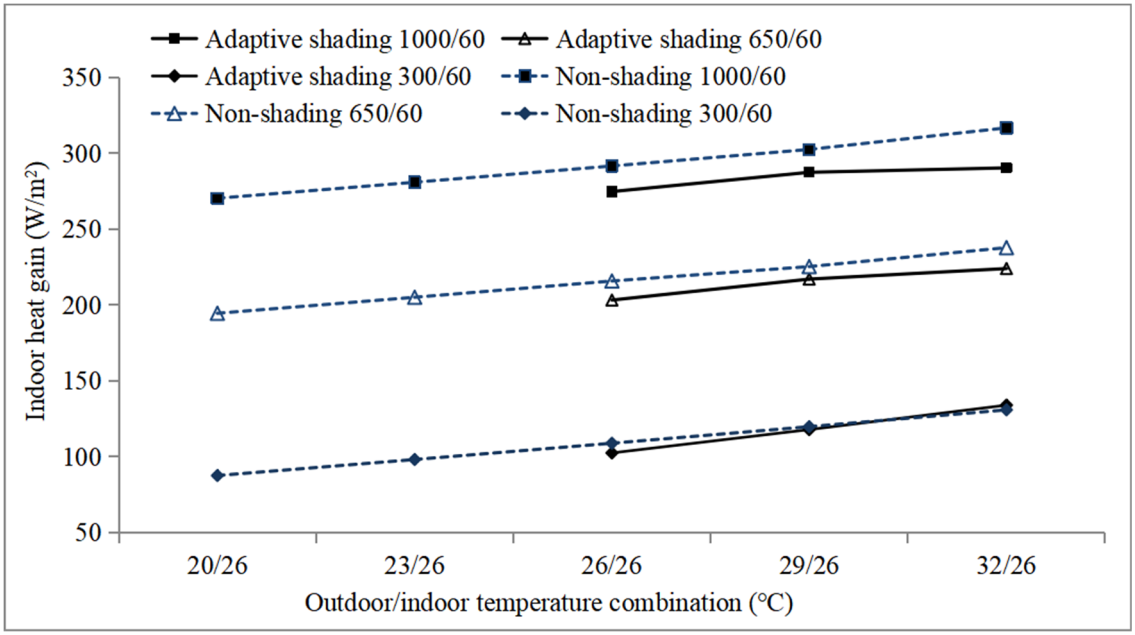

Figure 10. The total indoor heat gain through window under different outdoor/indoor temperature combinations.

In Figure 8, the solar transmission is shown to be influenced only by the incident angle and is unrelated to outdoor temperature for common triple-layer clear glass window. Therefore, the direct solar energy transmission through window under different ambient temperature remained the same (0.402) with constant incident angle (60°). For adaptive shading window, the direct solar energy transmission through window was reduced when ambient temperature exceeded 26 °C. The reduction was larger with stronger global solar irradiance and/or hotter ambient environment. With 1000, 650, and 300 W/m^2 global solar irradiance, the solar energy transmissions through the window were reduced from 240.0 W/m^2 to 200.5 W/m^2, from 177.7 W/m^2 to 151.5 W/m^2, and from 89.7 W/m^2 to 74.6 W/m^2, respectively, when outdoor temperature was 32 °C. The reduction percentages were approximately 16.0%. Meanwhile, the solar energy transmission reductions were from 240.0 W/m^2 to 211.8 W/m^2, from 177.7 W/m^2 to 156.8 W/m^2, and from 89.7 W/m^2 to 76.9 W/m^2, respectively, when outdoor temperature was 26 °C, with approximately 11.8% reduction.

Figure 9 illustrates the inward convective and radiative heat transfer from the innermost glass surface to indoor under different boundary conditions. The heat transfer was negative only when outdoor temperature was 20 °C and global solar irradiance was as weak as 300 W/m^2, representing an outward heat flow from indoor to ambient environment in this extreme condition. Accordingly, the window can be seen as a heat source for most of the time during the cooling season, even with surrounding temperature lower than indoor temperature. Therefore, the issue of solar shading should be taken into consideration for any air-conditioned rooms. For the common triple-layer clear glass window, the heat transfer increased from 30.4 W/m^2 to 76.9 W/m^2, i.e., by 2.5 times when outdoor temperature increased from 20 °C to 32 °C under the global solar irradiance level of 1000 W/m^2 and incident angle of 60°.

As mentioned above, there is no additional shading in the adaptive window when ambient temperature was below 26 °C, and its performance remained the same as the common triple-layer window. In practical applications, the window should be redesigned

according to the specific indoor air temperature. For example, if the preset temperature of indoor air temperature were 24 °C, the window should be designed to take action (provide liquid shading) when ambient temperature exceeds 24 °C. In this way, the indoor heat gain from ambient can be minimized to the largest extent and more cooling energy can be reduced. As for the present investigation, the window was designed on the basis of the 26 °C indoor temperature setting. This means, once the ambient temperature exceeded 26 °C, the shading liquid layer rose and, thus, caused a reduction of the comprehensive thermal insulation of the window, which resulted in a higher level of convective and radiative heat transfer to indoor. This is demonstrated in Figure 9, where black solid lines representing the adaptive shading window remained above the blue dotted lines.

It is worth noticing that the slopes of the black lines are steeper compared with the blue dotted lines when ambient temperature was between 26 °C and 29 °C. This indicates a critical heat transfer through the adaptive shading window with the additional liquid layer. However, when ambient temperature exceeded 29 °C, the slopes of the black lines became less steep when global irradiance was 1000 W/m^2 or 650 W/m^2. This was caused by the enhanced sun-blocking provided by higher level of shading liquid layer within the right-side window cavity, which reduced the amount of solar energy absorbed by the innermost glass pane. Therefore, the temperature increment of the inner glass pane was reduced, which slowed down the inward heat transfer. As for the 300 W/m^2 global irradiance level cases, the influence of solar radiation on inward heat transfer was less obvious.

The comprehensive indoor heat gains through window under different conditions were compared between the triple-layer clear glass window and the liquid-infill tunable window in Figure 10. It is obvious that the influence of shading liquid layer was positive for indoor cooling load reduction when solar radiation was strong. The liquid-infill tunable window permitted less heat to enter the air-conditioned room for most of the time. There was only one exception, which occurred with global irradiance level of 300 W/m^2 and incident angle of 30°, under 32 °C ambient temperature. These conditions represented hot and cloudy days. In summary, the heat gain reduction was within the range from 1.60% to 8.33% under other conditions, with average reduction percentage of 4.66%.

5. Discussion and Future Works

5.1. Discussion

As a low-cost energy-efficient window, the liquid-infill tunable window is capable of providing solar shading without additional energy consumption nor manual operation. The shading liquid layer rises to a higher level under stronger incident solar radiation and higher ambient temperature. According to the comparative simulation results, the indoor heat gain through this window can be reduced due to the additional shading provided by the colored liquid layer, though the comprehensive thermal insulation of the window actually decreased compared with the triple-layer glass window.

The comprehensive indoor heat gain through the liquid-infill tunable window is compared with other energy-efficient window designs. The thermal performance of water-flow window was presented in [34], in which the indoor heat gain was reduced from 380 W/m^2 to 314 W/m^2, i.e., reduced by 16.1%, while double-pane clear glass window was replaced with water-flow window under typical summer weather. The corresponding indoor heat gain reduction of the liquid-infill tunable window was 8.3% compared with the triple-pane clear glass window (from 316 W/m^2 to 290 W/m^2) under similar boundary conditions. The superior performance of water-flow window was obtained with a relatively complex system which utilized water flowing within the window cavity as a cooling medium, which would cause extra investment and maintenance. At the same time, the thermal performance of this liquid-infill tunable window was competitive compared with natural-ventilated window design in [35], through which indoor heat gain reduced from 184.0 W/m^2 to 172.5 W/m^2 during office hour, i.e., the average reduction rate was 6.25%. This is slightly higher compared with the liquid-infill tunable window under discussion,

which brought an average indoor heat gain decrease of 5.04%. However, considering additional sunshades are necessary for most natural-ventilated windows, which not only results in higher initial cost but also influences the heat removal effect of the flowing air within window cavity, the liquid-infill tunable window can be more attractive under certain circumstances.

On the other hand, better thermal performance can be anticipated if one or several of the clear glass panes are replaced with other types of glass. In [36], the total indoor heat gain from solar radiation decreased by 27% and 34% for a natural-ventilated slim double-skin window by replacing the clear glass with colored glass or low-e glass. Therefore, it is important to choose the appropriate type of glass with special properties while designing liquid-infill tunable windows in order to customize the thermal response and energy performance. Admittedly, the solar transmission of common double-pane glass windows is constant under the same solar incident angle, and extra solar shading device is always a necessity. Shading devices, fixed or adjustable, always bring about extra cost and maintenance, and the potential risk of falling objects. At the same time, though the cutting-edge electrochromic, thermochromic, or electrokinetic pixel windows can provide adaptive shading, the expensive price greatly restricts the extensive application [37,38].

In conclusion, the thermal performance of the liquid-infill tunable window under investigation is better for conditions with constant high ambient temperature and strong solar radiation. Considering the simple configuration and feasible materials involved, reasonable cost and short pay-back period is predictable.

On the other hand, it should be noted that there are several drawbacks which require rectifying, should the liquid-infill tunable window be applied in real projects:

(1) The loss of colored liquid due to volatilization and accompanied potential health risk must be taken into consideration. The working principle of liquid-infill tunable window requires the connection of colored liquid with the surrounding atmosphere. As illustrated in Figure 1, the shading liquid is actually exposed to the indoor air. This brings two risks: the loss of colored liquid in the long run because of volatilization, and the potential health risk to the building occupants.

(2) Uncomfortable sensation caused by asymmetric radiation from the window is another important issue. The smaller thermal insulation results in higher surface temperature of the innermost glass, which not only causes higher indoor heat gain through convective/radiative heat transfer, as pointed out in Section 4, but may also bring uncomfortable sensation caused by asymmetric radiation of indoor occupants, especially those close to the window.

(3) Directly transmitted solar radiation through the top part of liquid-infill tunable window should also be considered. The shading provided by the colored liquid is efficient, yet uneven. As demonstrated in Part 4, there is no shading liquid applied to the upper part of the window under most conditions. As a result, certain parts of the room might be warmed by the directly transmitted solar radiation.

(4) The liquid-infill tunable window under investigation was more suitable for regions with hot and long cooling seasons. However, in the heating season, the liquid within the window cavity might cause unfavorable heat loss from indoor to ambient environment through liquid heat conduction. There would be a heat bridge at the bottom of the window, which would influence the overall thermal performance. To amend this problem, it is better to design an evacuation hole at the bottom of the window frame so that the cavity can be emptied during the heating season.

5.2. Future Works

The above-mentioned problems should be investigated thoroughly before the liquid-infill tunable window can be extensively applied. Firstly, the colored liquid should be selected carefully. As mentioned in Section 3.1, multiple types of liquid materials might need to be mixed in order to achieve the required density as accurately as possible. This requires each component to be stable, non-volatile, non-toxic, and non-reactive with not

only other components but also the glass panes as well as the window frame. Meanwhile, the pigment or dye material within the liquid, if any, should also be stable and not prone to easily fade under long hours of solar irradiation. Moreover, a filter should be installed at the opening to prevent flies or bugs from accidentally entering the cavities.

Secondly, an additional glass pane and air layer can be applied as an improvement to the current design in order to solve the possible uncomfortable asymmetric radiation. The improved design is illustrated in Figure 11. The additional air layer on the right side provides thermal insulation to reduce inward heat transfer. The benefits include lessened risk of uncomfortable asymmetric radiation and reduced cooling load for the air-conditioning system.

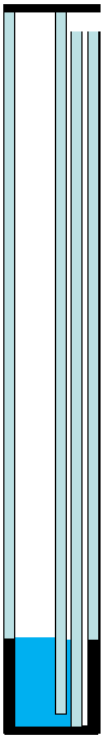

Figure 11. Improved design with additional glass pane and air layer.

An alternative choice is to utilize liquid materials with lower thermal conductivity. In this way, the inward heat transfer can be obstructed. Other types of glass panes, such as reflective glass, absorptive glass, or low-e glass, may also be selected as the innermost glass pane to achieve better thermal and energy performance, as discussed in Section 5.1. The effect of proposed improvements will be investigated in the next stage.

Thirdly, the improved design in Figure 12a can help to releive the problem of uneven solar transmission through the upper part of the window. The design employs two shading liquid layers (three window cavities in total) and can provide full coverage of solar block under relatively moderate conditions. The middle cavity is configured to be thinner, and the colored liquid flows to the right-side cavity after fulfilling the middle cavity, as presented in Figure 12b. When incident solar radiation weakens and/or ambient temperature decreases, the temperature and pressure of trapped air declines, which initiates the window to restore the initial state through a one-way valve at the bottom of the window, as demonstrated in Figure 12c. The shading liquid flows from the middle and the right-side cavities back to the bottom of the window. The performance of this improved design requires further investigation.

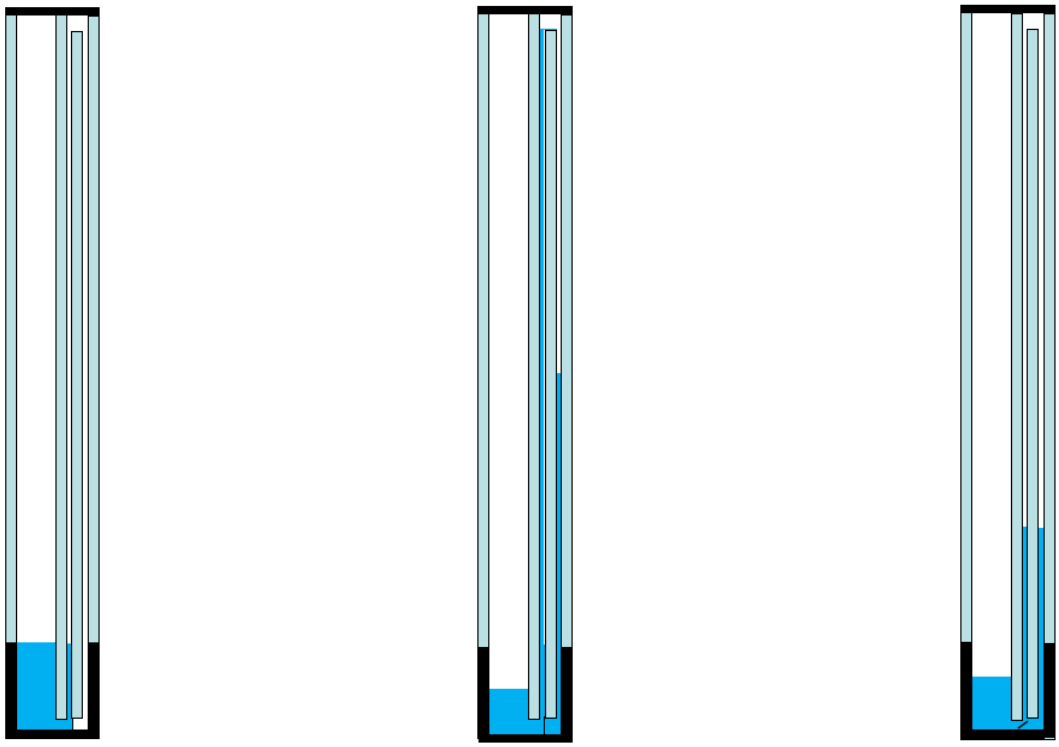

(**a**) (**b**) (**c**)

Figure 12. Improved design with double colored liquid layers. (**a**) Initial state. (**b**) Under strong solar radiation. (**c**) Restoring initial state.

6. Conclusions

Liquid-infill tunable window can provide flexible solar shading in accordance with the surrounding environment, which favors building energy-saving, especially in cooling-dominant regions. The main advantages include lower first investment, less maintenance labor, no risk of external sunshade falling, and better aesthetic outlook of the building.

In the present investigation, the numerical model of this compact energy-efficient window is set up, which can be inserted into building simulation tools. Its thermal performance is analyzed in comparison with triple-layer clear glass windows under different boundary conditions. The main findings include:

(1) The shading liquid layer in the window cavity is higher under stronger solar radiation or hotter environment, thus providing better sunshade. For the south-oriented window, the comprehensive solar transmissivity decreased by 16.0% and 11.8% with ambient temperature of 32 °C and 26 °C, respectively.

(2) Adversely, thermal insulation decreased since part of the air cavity is replaced with liquid within the liquid-infill tunable window. As a result, the indoor heat gain from convective/radiative heat transfer increased by more than 20%.

(3) The total indoor heat gain through the window is reduced within the range from 1.60% to 8.33% under different conditions, with average reduction percentage of 5.04% at the 60° incident angle. Better performance occurs under stronger solar radiation.

Overall, the liquid-infill tunable window is proven efficient in preventing excessive indoor heat gain from direct solar transmission. Further investigations are necessary to improve the comprehensive thermal insulation and solve the problems of uneven solar transmission and uncomfortable asymmetric radiation. The configuration and dimension of the window should be carefully decided in practice, with factors including local climate, building orientation, window size, building operation schedule, occupants' preference, privacy needs, and energy price taken into consideration.

Author Contributions: Methodology, C.L.; Software, X.L.; Investigation, X.W.; Writing—original draft, X.W.; Writing—review & editing, Y.Y.; Visualization, Y.Y.; Project administration, C.L. All authors have read and agreed to the published version of the manuscript.

Funding: The study was supported by the National Natural Science Foundation of China (Grant No. 52008254), Shenzhen Science and Technology Program (Project No. ZDSYS20210623101534001, JCYJ20210324093209025), and Research start-up fund for young teachers of Shenzhen University (Grant No. 20220429).

Institutional Review Board Statement: Not applicable.

Informed Consent Statement: Not applicable.

Conflicts of Interest: The authors declare no conflict of interest.

Nomenclature

A	*cross-sectional area*, m^2
d	thickness, m
G	solar radiation, W
g	gravitational constant, m/s^2
h	heat transfer coefficient, $W/(m^2 \cdot °C)$; height, m
L	length, m
P	pressure, Pa
T	temperature, $°C$
V	volume, m^3
W	width, m
Greek	
α	absorptivity, -
γ	reflectance, -
ε	emissivity, -
θ	absolute temperature, $°C$
ρ	density, kg/m^3
σ	Stefan–Boltzmann constant, 5.67×10^{-8} $W/(m^2 \cdot K^{-4})$
τ	transmittance, -
Subscripts	
0,1	the initial state and the transformed state
a	ambient; air
abs	absorptive
c	convective
g	glass
*g*1, *g*2, *g*3	numbers of glass panes
ref	reflective
r	radiative
rm	room
trans	transmitted
total	total
wind	wind
Superscript	
top	the top part of the window consisting of 3 layers of clear glass without liquid layer
lower	the lower part of the window consisting of 3 layers of clear glass with liquid layer in the cavity

References

1. Li, C.Z.; Zhang, L.; Liang, X.; Xiao, B.; Tam, V.W.Y.; Lai, X.; Chen, X. Advances in the research of building energy saving. *Energy Build.* **2022**, *254*, 111556. [CrossRef]
2. Guo, S.; Yan, D.; Hu, S.; Zhang, Y. Modelling building energy consumption in China under different future scenarios. *Energy* **2021**, *214*, 119063. [CrossRef]
3. Al-Masrani, S.M.; Al-Obaidi, K.M.; Zalin, N.A.; Isma, M.I.A. Design optimisation of solar shading systems for tropical office buildings: Challenges and future trends. *Sol. Energy* **2018**, *170*, 849–872. [CrossRef]

4. Carroll, M.K.; Anderson, A.M.; Mangu, S.T.; Hajjaj, Z.; Capron, M. Aesthetic Aerogel Window Design for Sustainable Buildings. *Sustainability* **2022**, *14*, 2887. [CrossRef]
5. Wu, H.; Zhang, T. Optimal design of complex dynamic shadings: Towards sustainable built environment. *Sustain. Cities Soc.* **2022**, *86*, 104109. [CrossRef]
6. Lyu, Y.; Chen, S.; Liu, C.; Li, J.; Li, C.; Su, H. Thermal Characteristics Simulation of an Energy-Conserving Facade: Water Flow Window. *Sustainability* **2022**, *14*, 2737. [CrossRef]
7. Manzan, M. Genetic optimization of external fixed shading devices. *Energy Build.* **2014**, *72*, 431–440. [CrossRef]
8. Hernández, F.F.; López, J.M.C.; Suárez, J.M.P.; Muriano, M.C.G.; Rueda, S.C. Effects of louvers shading devices on visual comfort and energy demand of an office building. A case of study. *Energy Procedia* **2017**, *140*, 207–216. [CrossRef]
9. Yao, J. An investigation into the impact of movable solar shades on energy, indoor thermal and visual comfort improvements. *Build. Environ.* **2014**, *71*, 24–32. [CrossRef]
10. Islam, N.; Irshad, K.; Zahir, H.; Islam, S. Numerical and experimental study on the performance of a Photovoltaic Trombe wall system with Venetian blinds. *Energy* **2021**, *218*, 119542. [CrossRef]
11. Tabadkani, A.; Roetzel, A.; Li, H.X.; Tsangrassoulis, A.; Attia, S. Analysis of the impact of automatic shading control scenarios on occupant's comfort and energy load. *Appl. Energy* **2021**, *294*, 116904. [CrossRef]
12. Karlsen, L.; Heiselberg, P.; Bryn, I.; Johra, H. Solar shading control strategy for office buildings in cold climate. *Energy Build.* **2016**, *118*, 316–328. [CrossRef]
13. da Silva, P.C.; Leal, V.; Andersen, M. Occupants interaction with electric lighting and shading systems in real single-occupied offices: Results from a monitoring campaign. *Build. Environ.* **2013**, *64*, 152–168. [CrossRef]
14. O'Brien, W.; Kapsis, K.; Athienitis, A.K. Manually-operated window shade patterns in office buildings: A critical review. *Build. Environ.* **2013**, *60*, 319–338. [CrossRef]
15. Casini, M. Active dynamic windows for buildings: A review. *Renew. Energy* **2018**, *119*, 923–934. [CrossRef]
16. Rezaei, S.D.; Shannigrahi, S.; Ramakrishna, S. A review of conventional, advanced, and smart glazing technologies and materials for improving indoor environment. *Sol. Energy Mater. Sol. Cells* **2017**, *159*, 26–51. [CrossRef]
17. Ye, H.; Long, L.; Zhang, H.; Gao, Y. The energy saving index and the performance evaluation of thermochromic windows in passive buildings. *Renew. Energy* **2014**, *66*, 215–221. [CrossRef]
18. DeForest, N.; Shehabi, A.; Selkowitz, S.; Milliron, D.J. A comparative energy analysis of three electrochromic glazing technologies in commercial and residential buildings. *Appl. Energy* **2017**, *192*, 95–109. [CrossRef]
19. Cupelli, D.; Nicoletta, F.P.; Manfredi, S.; Vivacqua, M.; Formoso, P.; De Filpo, G.; Chidichimo, G. Self-adjusting smart windows based on polymer-dispersed liquid crystals. *Sol. Energy Mater. Sol. Cells* **2009**, *93*, 2008–2012. [CrossRef]
20. Ghosh, A.; Norton, B.; Duffy, A. Daylighting performance and glare calculation of a suspended particle device switchable glazing. *Sol. Energy* **2016**, *132*, 114–128. [CrossRef]
21. Li, X.H.; Liu, C.; Feng, S.P.; Fang, N.X. Broadband light management with thermochromic hydrogel microparticles for smart windows. *Joule* **2019**, *3*, 290–302. [CrossRef]
22. Zhu, H.; Wang, L. Smart window based on Cu7S4/hydrogel composites with fast photothermal response. *Sol. Energy Mater. Sol. Cells* **2019**, *202*, 110109. [CrossRef]
23. Jiang, T.; Zhao, X.; Yin, X.; Yang, R.; Tan, G. Dynamically adaptive window design with thermo-responsive hydrogel for energy efficiency. *Appl. Energy* **2021**, *287*, 116573. [CrossRef]
24. Aburas, M.; Ebendorff-Heidepriem, H.; Lei, L.; Li, M.; Zhao, J.; Williamson, T.; Wu, Y.; Soebarto, V. Smart windows—Transmittance tuned thermochromic coatings for dynamic control of building performance. *Energy Build.* **2021**, *235*, 110717. [CrossRef]
25. Nakamura, A.; Ogai, R.; Murakami, K. Development of smart window using an hydroxypropyl cellulose-acrylamide hydrogel and evaluation of weathering resistance and heat shielding effect. *Sol. Energy Mater. Sol. Cells* **2021**, *232*, 111348. [CrossRef]
26. Gil-Lopez, T.; Gimenez-Molina, C. Influence of double glazing with a circulating water cavity on the thermal energy savings in buildings. *Energy Build.* **2013**, *56*, 56–65. [CrossRef]
27. Lyu, Y. *A Liquid Medium Energy Saving Window Technique and Application*; Metallurgical Industry Press: Beijing, China, 2020.
28. Li, C.; Tang, H.; Tan, J.; Li, C.; Yang, Y.; Zeng, F. Numerical simulation on year-round performance of water-flow window with different shading control modes. *Build. Serv. Eng. Res. Technol.* **2020**, *42*, 157–174. [CrossRef]
29. Fazel, A.; Izadi, A.; Azizi, M. Low-cost solar thermal based adaptive window: Combination of energy-saving and self-adjustment in buildings. *Sol. Energy* **2016**, *133*, 274–282. [CrossRef]
30. Watmuff, J.H.; Charters WW, S.; Proctor, D. Solar and wind induced external coefficients-solar collectors. *Coop. Mediterr. Pour L'energie Sol.* **1977**, 56. Available online: https://www.researchgate.net/publication/234355019_Solar_and_wind_induced_external_coefficients_-_Solar_collectors (accessed on 30 June 2022).
31. LBNL Window. Available online: https://windows.lbl.gov/software/window (accessed on 30 June 2022).
32. Chunying, L. Performance Evaluation of Water-Flow Window Glazing. Ph.D. Thesis, City University of Hong Kong, Hong Kong, China, 2012.
33. Duffie, J.A.; Beckman, W.A. *Solar Engineering of Thermal Processes*; John Wiley & Sons: Hoboken, NJ, USA, 2013.
34. Chow, T.T.; Li, C.; Lin, Z. The function of solar absorbing window as water-heating device. *Build. Environ.* **2011**, *46*, 955–960. [CrossRef]

35. Chow, T.T.; Li, C.; Lin, Z.; Fong, K.F.; Chan, L.S.; Pei, G. Experimental evaluation of ventilated glazing performance in Hong Kong. *Int. J. Energy Res.* **2009**, *33*, 526–537. [CrossRef]
36. Choi, H.; An, Y.; Kang, K.; Yoon, S.; Kim, T. Cooling energy performance and thermal characteristics of a naturally ventilated slim double-skin window. *Appl. Therm. Eng.* **2019**, *160*, 114113. [CrossRef]
37. Tällberg, R.; Jelle, B.P.; Loonen, R.; Gao, T.; Hamdy, M. Comparison of the energy saving potential of adaptive and controllable smart windows: A state-of-the-art review and simulation studies of thermochromic, photochromic and electrochromic technologies. *Sol. Energy Mater. Sol. Cells* **2019**, *200*, 109828. [CrossRef]
38. Aburas, M.; Soebarto, V.; Williamson, T.; Liang, R.; Ebendorff-Heidepriem, H.; Wu, Y. Thermochromic smart window technologies for building application: A review. *Appl. Energy* **2019**, *255*, 113522. [CrossRef]